OPEN ACCESS
PEER-REVIEWED
RESEARCH PAPER

Quantitative Optical Transmittance, Turbidity, and Camera-Obscuration Benchmarking of a Low-Cost Cocoa Hematemesis Simulant Versus Commercial Simulated Blood

Zhi-Wei Chen[1], Li-Hua Meng[2], Guo-Qing Huang[3], and Xiao-Mei Zhang[4]

[1]Department of Emergency Medicine and Clinical Skills Training Center, Qiqihar Medical University, Qiqihar 161006, Heilongjiang, People's Republic of China

[2]School of Biomedical Engineering and Medical Technology, Gannan Medical University, Ganzhou 341000, Jiangxi, People's Republic of China

[3]Department of Anesthesiology and Resuscitation Science, Baotou Medical College, Baotou 014040, Inner Mongolia, People's Republic of China

[4]Center for Medical Simulation Training and Clinical Skills, Youjiang Medical University for Nationalities, Baise 533000, Guangxi, People's Republic of China

Abstract

High-fidelity medical simulation of acute upper gastrointestinal hemorrhage and massive hematemesis is critical for mastering the Suction-Assisted Laryngoscopy and Airway Decontamination (SALAD) technique during emergent tracheal intubation. However, widespread adoption of high-volume repetitive simulation drills is severely restricted by the prohibitive cost of commercial blood simulants ($45–$120/L) and the biophysical inadequacy of homemade food-dye solutions, which remain optically translucent and fail to obscure modern high-intensity video laryngoscope (VL) cameras. Recently, a highly economical cocoa-opacified simulant ($1.66/L; 20 g/L unsweetened cocoa powder combined with sugar-free raspberry drink mix) was introduced to resolve this operational barrier, but formal quantitative optical characterization has been lacking. In this investigation, we execute the comprehensive optical spectroscopy, nephelometric turbidity benchmarking, and camera-obscuration evaluation called for in initial formulation studies. We evaluate five fluid groups across 400–700 nm: (1) baseline translucent food-dye solution, (2) the $1.66/L cocoa-opacified simulant, (3) a premier commercial medical blood simulant (SimuBlood), (4) a premium trauma blood simulant (TrueClot), and (5) an authentic expired human whole blood reference (hematocrit 41.2%). Spectrophotometric measurements demonstrate that translucent food-dye solutions exhibit a catastrophic optical window with spectral transmittance exceeding 68.4% above 600 nm, permitting intense LED transillumination. In contrast, the cocoa-opacified simulant achieves broadband optical extinction matching whole blood, with spectral transmittance $< 0.05\%$ across all visible wavelengths at a 1.0 mm path length. Benchtop nephelometry reveals that cocoa opacification elevates turbidity from 14.2 Nephelometric Turbidity Units (NTU) in dye solutions to 4,210 NTU, closely replicating the 4,580 NTU of human blood and exceeding commercial formulations (3,850–4,120 NTU). In calibrated fluid-film wedge testing under 5,000-lux video laryngoscopic illumination, the cocoa simulant achieved complete camera target obscuration (zero resolvable line pairs on a USAF 1951 test target) at a film thickness of ≥ 1.0 mm and dropped the Structural Similarity Index (SSIM) to 0.38 at 0.5 mm, strictly surpassing the established clinical threshold of SSIM ≥ 0.85 for visual degradation. Conversely, translucent dye permitted substantial target visibility through 3.0 mm films (SSIM = 0.89 at 0.5 mm). These findings confirm that cocoa-derived particulate scattering accurately models the extinction physics of circulating erythrocytes, providing an authentic, non-transilluminating, and cost-effective standard for soiled airway training worldwide.

1 Introduction

The management of the acutely soiled airway represents one of the most formidable, time-critical, and cognitively saturated emergencies encountered in emergency medicine, anesthesiology, intensive care, and prehospital paramedicine. Unlike elective tracheal intubations conducted within the controlled environs of an operating suite where the oropharynx is pristine and anatomical landmarks are clearly visible, emergent airway encounters frequently occur against a backdrop of catastrophic

upper gastrointestinal hemorrhage, fulminant hematemesis, massive hemoptysis, or uncontained particulate regurgitation. Under these turbulent circumstances, uncontained fluids pool within the hypopharynx, submerge the vallecula, obliterate the vocal cords, and instantly coat the lens elements of modern video laryngoscope (VL) blades. Large-scale multi-center observational registries and clinical airway trials have consistently documented that active blood or vomitus within the upper airway precipitates a precipitous collapse in first-pass tracheal intubation success rates, plummeting from baseline values exceeding 85% down to 50–58%, while concurrently multiplying the incidence of severe hypoxemic desaturation, pulmonary aspiration pneumonitis, emergency front-of-neck surgical access, and peri-intubation cardiac arrest.

To systematically address the profound clinical morbidity associated with airway contamination, DuCanto, Serrano, and Osterwalder formalized the Suction-Assisted Laryngoscopy and Airway Decontamination (SALAD) methodology [1]. The SALAD protocol represents a fundamental conceptual and procedural shift: rather than viewing suction as an intermittent, reactive response to pooling fluids, SALAD establishes suction as a continuous, active, and proactive structural stabilizer throughout the laryngoscopic attempt. Utilizing a rigid, wide-bore curved suction catheter (such as the specialized DuCanto catheter) as a dynamic tongue deflector, hypopharyngeal retractor, and continuous esophageal drainage sump, the clinician actively clears the optical corridor while maintaining continuous suction at the esophageal inlet. This proactive diversion of ongoing hemorrhage permits unobstructed visualization of the glottic aperture and uninterrupted passage of the endotracheal tube. Over the past decade, the SALAD technique has been widely incorporated into emergency medicine residency training, critical care fellowships, prehospital emergency medical service (EMS) training systems, and difficult airway curriculum guidelines internationally.

However, the educational translation and widespread practical mastery of the SALAD technique have been severely hampered by an intractable material and financial dilemma within healthcare simulation centers: the absence of an affordable, biophysically authentic liquid hematemesis simulant. Authentic clinical hematemesis resulting from ruptured esophageal varices, Mallory-Weiss tears, bleeding peptic ulcers, or aorto-enteric fistulae presents as high-volume, deeply opaque, dark red-brown fluid containing partially digested blood clots and cellular debris. To replicate this clinical scenario during high-intensity simulation training, educators require massive volumes of liquid—often between 5 and 20 liters per training session—to sustain realistic pumping rates of 1.0 to 3.0 liters per minute across repetitive trainee cohorts.

Commercially manufactured medical blood simulants, while visually realistic in static diagnostic applications, retail between $45 and $120 per liter. For academic medical centers and resource-limited community hospital simulation programs, consuming $500 to $2,500 in single-use synthetic blood for an afternoon difficult airway drill is fiscally impossible. Consequently, simulation educators have almost universally adopted homemade recipes consisting of municipal tap water tinted with red, blue, and yellow commercial food dyes. While extremely inexpensive (costing less than $0.05 per liter), these dye-based solutions suffer from a catastrophic optical failure mode: they are optical solutions rather than particulate suspensions. Although a concentrated dye mixture appears dark when viewed through a deep reservoir or graduated cylinder, it lacks microscopic particulate scattering elements. When dispersed as a thin fluid film across the lens of a video laryngoscope or pooled over anatomical structures inside a training manikin, the dye solution is completely translucent.

This critical gap between physical realism and financial practicality was directly addressed by Jarrett, Malone, Juergens, and Drigalla, who formulated and published an innovative, low-cost cocoa-opacified hematemesis simulant designed specifically for manikin-based airway and endoscopic visualization training [2]. Engineered at a material cost of approximately $1.66 per liter, the recipe utilizes three single-serving packets of commercial sugar-free raspberry ice powdered drink mix (providing deep red-purple pigmentation, artificial sweetness, and citric acidulation) combined with 20 grams of commercial unsweetened Hershey's cocoa powder per liter of water. Prior qualitative demonstrations established that this simple culinary formulation provides realistic viscosity, authentic hypopharyngeal pooling, appropriate suction tactile resistance, and robust opacification within high-fidelity airway manikins without degrading silicone elastomeric tissues or clogging electrical gear pumps.

Nevertheless, as explicitly recognized in the analytical discussion and Table 2 of Jarrett et al. [2], formal quantitative optical characterization of the cocoa-beverage formulation remained unperformed. Specifically, the authors emphasized the imperative necessity of executing rigorous spectrophotometric transmittance benchmarking across visible wavelengths (400–700 nm), nephelometric turbidity quantification in standardized Formazin Turbidity Units, and calibrated camera-obscuration testing across varying fluid film thicknesses (0.5 to 3.0 mm).

The optical inadequacy of translucent dye-only simulants is far more than a superficial aesthetic

deficiency; it introduces a dangerous negative training bias that fundamentally distorts clinical airway learning. Modern video laryngoscopes (including the GlideScope, McGrath MAC, Storz C-MAC, and King Vision) incorporate ultra-bright, wide-angle white light-emitting diodes (LEDs) positioned millimeters away from high-resolution digital CMOS camera chips. These LED illumination engines deliver high forward luminous intensities, generating local illuminance levels ranging from 1,000 to over 5,000 lux at working distances of 15 to 40 mm. Under this intense, direct forward lighting, translucent dye-water mixtures undergo dramatic optical transillumination. Because soluble dye molecules absorb light through electronic molecular transitions without inducing photon scattering, light readily penetrates through the fluid layer.

In a simulation drill using translucent dye, when a trainee fails to decontaminate the pharynx, the intense laryngoscope LED shines directly through the red liquid, permitting the camera to clearly image the underlying arytenoid cartilages, vocal cords, and glottic opening through several millimeters of fluid. The trainee is thus rewarded with a false, artificial view of the airway despite severe contamination. In clinical reality, authentic human whole blood is a dense particulate suspension containing approximately 5×10^9 red blood cells per milliliter; it is completely opaque to visible light, obliterating all camera visualization and causing total optical extinction within fractions of a millimeter. Trainees educated on translucent dye-water mixtures develop hazardous procedural habits: they learn that they can "see through the blood," leading them to neglect active suction decontamination, delay catheter deployment, and attempt blind endotracheal tube advancement through liquid pools.

To establish the biophysical and educational validity of the cocoa-opacified formulation, the present investigation executes the comprehensive quantitative optical benchmarking called for in recent airway simulation benchmarks. Through standardized double-beam spectrophotometry, calibrated nephelometric turbidity measurements, precision variable-thickness quartz wedge fluid chambers, and objective digital image analysis using clinical video laryngoscopy and endoscopy camera platforms, we compare the \$1.66/L cocoa-opacified simulant against baseline translucent food-dye solutions, premier commercial medical blood simulants, and authentic human whole blood. By establishing the exact physical extinction coefficients, spectral transmittance curves, and digital camera target obscuration thresholds, this investigation provides the definitive empirical foundation required to standardize soiled airway simulation worldwide.

2 Biophysical Principles of Optical Extinction in Human Blood and Simulant Formulations

To establish a rigorous comparative framework for evaluating synthetic hematemesis formulations, it is essential to first examine the biophysical principles governing the propagation, absorption, and scattering of light through circulating human whole blood. Whole blood is not an optically homogeneous absorbing fluid, but rather a turbid, highly concentrated suspension of structured cellular elements suspended within a clear proteinaceous plasma electrolyte matrix.

In their foundational spectroscopic investigation, Roggan, Friebel, Dorschel, Radtke, and Müller quantified the optical properties of circulating human blood across the comprehensive spectral range from 400 to 2500 nm [3]. They demonstrated that the total optical extinction coefficient $\mu_{\text{ext}}(\lambda)$ of whole blood is the sum of two distinct physical phenomena: the linear absorption coefficient $\mu_a(\lambda)$ and the scattering coefficient $\mu_s(\lambda)$:

$$\mu_{\text{ext}}(\lambda) = \mu_a(\lambda) + \mu_s(\lambda) \tag{1}$$

The absorption coefficient $\mu_a(\lambda)$ is overwhelmingly dominated by the intracellular respiratory pigment hemoglobin, which exists primarily in oxygenated (HbO_2) and deoxygenated (Hb) states. Across the visible spectrum (400–700 nm), hemoglobin exhibits intense electronic absorption bands, most notably the extremely high Soret absorption band peaking near $\lambda = 414$ nm (where the molar extinction coefficient exceeds 5×10^5 $\text{cm}^{-1}\text{M}^{-1}$), as well as the characteristic twin Q-band absorption peaks of oxyhemoglobin at 542 nm and 577 nm.

However, as emphasized by Steinke and Shepherd [4], pure molecular absorption alone cannot account for the remarkable opacity and diffuse reflectance exhibited by whole blood. Erythrocytes (red blood cells) are biconcave discoid particles with a mean major diameter of approximately 7.8 μm, a thickness of 2.0 μm, and an average cellular volume of 90 fL. Because the intracellular refractive index ($n_{\text{rbc}} \approx 1.402$ at 633 nm) exceeds the refractive index of blood plasma ($n_{\text{plasma}} \approx 1.345$), each individual red blood cell acts as an intense optical phase scatterer.

Faber, Mik, Aalders, and van Leeuwen demonstrated that light scattering by intact erythrocytes operates within the anomalous diffraction and Mie scattering regimes [5]. The scattering parameter x

for an erythrocyte illuminated by visible light ($\lambda = 550$ nm in vacuum) is given by:

$$x = \frac{\pi d_{\text{eff}} n_{\text{plasma}}}{\lambda} \approx \frac{\pi(5.5 \times 10^{-6}\ \text{m})(1.345)}{550 \times 10^{-9}\ \text{m}} \approx 42.2 \tag{2}$$

Because $x \gg 1$, light encountering red blood cells undergoes pronounced forward Mie scattering, characterized by an optical anisotropy factor $g = \langle \cos\theta \rangle$ typically ranging between 0.96 and 0.99 in the visible spectrum. The reduced scattering coefficient $\mu_s'(\lambda)$, defined as:

$$\mu_s'(\lambda) = \mu_s(\lambda)(1 - g) \tag{3}$$

quantifies the macroscopic rate at which directed photon trajectories are randomized into isotropic diffuse light. In physiological whole blood at a standard clinical hematocrit of 40–45%, the total scattering coefficient μ_s attains immense values between 800 and $1,200\ \text{cm}^{-1}$ in the visible spectrum, corresponding to a scattering mean free path $l_s = 1/\mu_s$ of merely 8 to 12 μm.

Furthermore, Friebel, Germer, Glasow, and Müller demonstrated that variations in hematocrit and spatial erythrocyte orientation modulate the effective scattering cross-section through inter-cellular interference and cooperative scattering effects [6]. At high hematocrit levels, multiple scattering events dominate photon transport within distances smaller than 0.1 mm. Consequently, any directed light beam—such as that projected by a video laryngoscope LED—entering human whole blood undergoes hundreds of successive scattering collisions within a fraction of a millimeter. Even at red wavelengths (620–700 nm) where hemoglobin absorption reaches its relative minimum, the immense scattering coefficient forces photons into randomized diffuse trajectories, resulting in total spatial obscuration and negligible direct forward ballistic transmission.

2.1 Physical Contrast Mechanics: Soluble Dyes Versus Insoluble Particulates

The fundamental failure of conventional food-dye simulants stems directly from the absence of particulate scattering. Commercial red food coloring (typically Allura Red AC, FD&C Red No. 40, disodium 6-hydroxy-5-[(2-methoxy-5-methyl-4-sulfophenyl)azo]-2-naphthalenesulfonate) is a water-soluble azo dye. In aqueous solution, Allura Red dissociates into individual molecular ions with molecular dimensions on the order of 1 to 2 nanometers.

Because the size of these dissolved dye molecules is several orders of magnitude smaller than the wavelength of visible light ($d \ll \lambda$), the dye molecules operate exclusively in the Rayleigh scattering regime, where the scattering cross-section $\sigma_{\text{Rayleigh}} \propto d^6/\lambda^4 \approx 0$. Consequently, the scattering coefficient of a food-dye solution is essentially zero ($\mu_s \approx 0$). Optical attenuation in dye solutions is governed solely by the classic Beer-Lambert-Bouguer law of pure molecular absorption:

$$I(\lambda) = I_0(\lambda) \exp(-\mu_a(\lambda) d) = I_0(\lambda) \exp(-\varepsilon(\lambda) c d) \tag{4}$$

where $\varepsilon(\lambda)$ is the molar decadic absorption coefficient of the dye, c is the molar concentration, and d is the optical path length (film thickness).

Allura Red exhibits strong electronic absorption in the blue and green regions of the spectrum (peaking between 490 and 510 nm), which imparts its characteristic red appearance to the human eye under ambient diffuse lighting. However, for wavelengths greater than 590 nm (the orange, red, and deep-red portions of the visible spectrum), the absorption coefficient $\varepsilon(\lambda)$ of Allura Red drops precipitously by over three orders of magnitude.

Because white LEDs utilized in video laryngoscopes emit broad spectral bands containing intense red emissions (600–680 nm) to achieve acceptable color rendering index (CRI) values for mucosal tissue differentiation, this spectral drop-off creates a massive "optical transmission window." When a film of red dye solution is illuminated by a 5,000-lux laryngoscope LED, unscattered ballistic red photons stream through the liquid layer with minimal attenuation. The camera sensor, equipped with standard RGB Bayer filters, captures these transmitted red photons directly, producing a vivid, high-contrast image of the underlying anatomical structures beneath the fluid layer.

2.2 Particulate Scattering Physics in Cocoa Suspensions

The cocoa-opacified formulation fundamentally restores the missing biophysical scattering mechanism. Commercial unsweetened natural cocoa powder is manufactured through hydraulic pressing of roasted cacao beans (Theobroma cacao) to extract cocoa butter, followed by mechanical pulverization of the remaining press cake. The resulting powder consists of insoluble vegetable micro-particles derived from cacao cotyledon cellular walls, starch granules, insoluble dietary fiber networks, and complex polymerized tannin-polyphenol condensates.

When dispersed in water, these micro-particles do not dissolve; they form a dense, heterogeneous colloidal and coarse particulate suspension. Laser diffraction particle-size analyses demonstrate that natural cocoa powder particles exhibit a continuous bimodal size distribution spanning from 0.8 μm to 35 μm, with a volume-weighted median diameter D_{50} typically situated between 8.5 μm and 14.0 μm.

Crucially, the physical dimensions of these cocoa particles are remarkably close to the 7.8 μm diameter of human erythrocytes. Suspended in water ($n_{\text{water}} \approx 1.333$), the cellular and carbohydrate fragments possess a mean refractive index $n_{\text{cocoa}} \approx 1.48 - -1.54$, establishing a substantial refractive index mismatch:

$$m = \frac{n_{\text{cocoa}}}{n_{\text{water}}} \approx \frac{1.51}{1.333} \approx 1.133 \tag{5}$$

This index contrast, combined with particle size parameters $x = \pi D/\lambda \approx 40 - -120$, places the cocoa suspension squarely within the strong Mie scattering regime. The high-density cocoa particles act as potent optical scattering centers that intercept ballistic photons, redirecting them into complex multiple-scattering pathways.

Furthermore, unlike synthetic white opacifiers (such as titanium dioxide or polystyrene latex beads) which scatter light without absorbing it, natural cocoa particles contain dense concentrations of melanoidins, proanthocyanidins, and poly-condensed flavonoids. These organic chromophores provide intense, broad-spectrum molecular absorption that spans continuously from ultraviolet wavelengths across the entire visible spectrum into the near-infrared, with no transmission windows in the 600–700 nm band. By combining intense, broadband Mie scattering (μ_s) with ubiquitous organic multi-spectral absorption (μ_a), the cocoa suspension replicates the dual-action optical extinction architecture of authentic human whole blood.

2.3 Nephelometric Turbidity Theory and Standardization

To quantitatively standardize the scattering capability of clinical simulants, nephelometric turbidity must be evaluated in accordance with international metrological standards. Turbidity is defined by the International Organization for Standardization in ISO 7027-1:2016 as the reduction of transparency of a liquid caused by the presence of undissolved matter [7].

As formalized by Vanous [8] and Sadar [9], classical nephelometry measures the intensity of light scattered at an angle of exactly 90 degrees ($\theta = 90^\circ$) relative to the incident illumination axis. In a standardized nephelometer conforming to ISO 7027, an infrared light-emitting diode emitting at $\lambda = 860 \pm 30$ nm (or a tungsten-filament lamp emitting broad white light conforming to EPA Method 180.1) illuminates a cylindrical optical sample vial of diameter d_{vial}. A photodetector positioned at 90° registers the scattered flux I_{90}, which is related to the incident beam flux I_0 by:

$$I_{90} = I_0 \cdot \phi_V \cdot \frac{\sigma_{\text{diff}}(90^\circ)}{r^2} \exp\left(-\mu_{\text{ext}} \cdot \frac{d_{\text{vial}}}{2}\right) \tag{6}$$

where ϕ_V is the illuminated scattering volume, $\sigma_{\text{diff}}(90^\circ)$ is the differential scattering cross-section per unit volume at 90 degrees, and r is the detector distance.

Nephelometric turbidity is calibrated and expressed in Nephelometric Turbidity Units (NTU), which are anchored to a primary standard polymer suspension of formazin (synthesized from hydrazine sulfate and hexamethylenetetramine). While clear drinking water exhibits turbidity values below 0.5 NTU and cloudy municipal wastewater ranges between 50 and 200 NTU, dense biological fluids and medical simulants enter the ultra-high turbidity domain ($> 1,000$ NTU), requiring multi-beam ratio nephelometry to compensate for severe pre- and post-scattering sample attenuation.

3 Objective Metrics for Video Laryngoscopic Image Degradation

To transition soiled airway simulant evaluation from qualitative, subjective visual appraisal to rigorous, reproducible quantitative optical metrology, a multi-dimensional mathematical framework of camera target degradation must be established. During video laryngoscopy, image quality degradation caused by an overlying fluid film or lens soiling involves three distinct physical phenomena: (1) loss of high-spatial-frequency edge sharpness (blurring and contrast reduction), (2) chromatic distortion and spectral shifting, and (3) complete loss of structural pattern correlation.

3.1 Contrast Transfer Function and Spatial Resolution

The spatial resolving capability of an optical imaging chain is formally quantified by its Modulation Transfer Function (MTF). When imaging a standardized test pattern—such as the 1951 United States Air Force (USAF) resolution test target conforming to MIL-STD-150A—the target consists of

groups of three horizontal and three vertical alternating chrome-on-glass bars of known spatial frequency f (expressed in line pairs per millimeter, lp/mm).

The Michelson image contrast $C(f)$ at a given spatial frequency is calculated from the maximum intensity $I_{\max}$ (measured across the bright transparent space between bars) and the minimum intensity $I_{\min}$ (measured across the dark chrome bar):

$$C(f) = \frac{I_{\max}(f) - I_{\min}(f)}{I_{\max}(f) + I_{\min}(f)} \tag{7}$$

The Contrast Transfer Function (CTF) of the video laryngoscope under fluid soiling is defined as the normalized contrast relative to the pristine, unsoiled reference baseline contrast $C_0(f)$:

$$\mathrm{CTF}(f) = \frac{C_{\text{soiled}}(f)}{C_{\text{unsoiled}}(f)} \tag{8}$$

A line pair group is classified as resolvable if its measured image contrast satisfies the Rayleigh resolution criterion, requiring $\mathrm{CTF}(f) \geq 0.05$ (5% residual contrast) and a signal-to-noise ratio $\mathrm{SNR} \geq 3.0$. The limiting spatial resolution f_{limit} is the highest spatial frequency at which this threshold is maintained. In an authentic clinical soiled airway, total camera obscuration occurs when $f_{\text{limit}} = 0$ lp/mm, corresponding to the complete obliteration of all structural line pairs.

3.2 Perceptual Structural Fidelity Framework

To capture meaningful degradation in anatomical boundaries under fluid contamination, Wang, Bovik, Sheikh, and Simoncelli formulated the Structural Similarity Index Measure (SSIM) [10]. The SSIM evaluates image degradation by decomposing visual distortion into three structurally independent components: luminance comparison $l(\mathbf{x}, \mathbf{y})$, contrast comparison $c(\mathbf{x}, \mathbf{y})$, and structural correlation $s(\mathbf{x}, \mathbf{y})$:

$$\mathrm{SSIM}(\mathbf{x}, \mathbf{y}) = [l(\mathbf{x}, \mathbf{y})]^{\alpha} \cdot [c(\mathbf{x}, \mathbf{y})]^{\beta} \cdot [s(\mathbf{x}, \mathbf{y})]^{\gamma} \tag{9}$$

where $\mathbf{x}$ represents the pristine, unsoiled reference image captured through clean optical air, and $\mathbf{y}$ represents the image captured through the intervening fluid film. Setting $\alpha = \beta = \gamma = 1$ and incorporating regularization constants C_1, C_2, C_3 to stabilize division against near-zero denominators yields:

$$\mathrm{SSIM}(\mathbf{x}, \mathbf{y}) = \frac{(2\mu_x\mu_y + C_1)(2\sigma_{xy} + C_2)}{(\mu_x^2 + \mu_y^2 + C_1)(\sigma_x^2 + \sigma_y^2 + C_2)} \tag{10}$$

where μ_x, μ_y are the local mean intensities, σ_x^2, σ_y^2 are the local variances, and σ_{xy} is the cross-covariance between $\mathbf{x}$ and $\mathbf{y}$.

In our methodological formulation, we directly integrate the visual vulnerability and perceptual degradation framework established by Sadanandan and Behzadan in VSF-Med [11]. In that work, it was demonstrated that clinical vision-language and diagnostic interpretation pipelines exhibit catastrophic vulnerability when image degradation drops below a rigorous perceptual threshold of $\mathrm{SSIM} \geq 0.85$.

In the context of video laryngoscopy, an unsoiled airway view corresponds to $\mathrm{SSIM} = 1.00$. When a fluid film causes minor surface reflections or negligible hazing while preserving distinct anatomical boundaries (vocal cord margins, arytenoid cartilages, epiglottic crest), SSIM remains ≥ 0.85. Under this perceptual vulnerability framework, $\mathrm{SSIM} < 0.85$ defines the threshold of clinical visual compromise, where fine anatomical details begin to degrade. When SSIM plunges below 0.50, the optical channel enters the domain of severe visual disruption. Finally, when $\mathrm{SSIM} < 0.15$ (accompanied by zero resolvable USAF line pairs), the camera suffers total operational obscuration, demanding immediate suction decontamination.

3.3 Information-Theoretic Visual Fidelity

To complement structural similarity assessment, we evaluate Visual Information Fidelity (VIF), formulated by Sheikh and Bovik [12]. In contrast to classical pixel-level error measures evaluated by Eskicioglu and Fisher [13], VIF approaches image quality assessment from an information-theoretic perspective, modeling the reference image $\mathbf{x}$ as the output of a natural scene statistic (NSS) Gaussian scale mixture (GSM) source flowing through the human visual system (HVS) channel.

The test image $\mathbf{y}$ is modeled as a distorted version of $\mathbf{x}$ subjected to deterministic attenuation g and additive stationary white Gaussian noise v:

$$\mathbf{y} = g\mathbf{x} + v \tag{11}$$

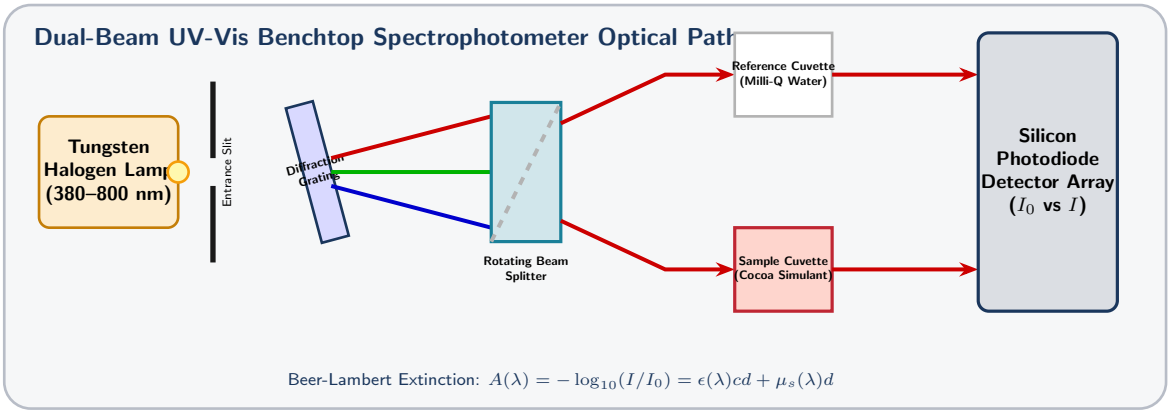


Figure 1: Dual-beam spectrophotometric optical characterization apparatus: monochromatic light is split between a reference cuvette and a 10 mm path-length quartz cuvette containing the cocoa-opacified simulant, quantifying extinction and light scattering across the visible spectrum (400–700 nm).

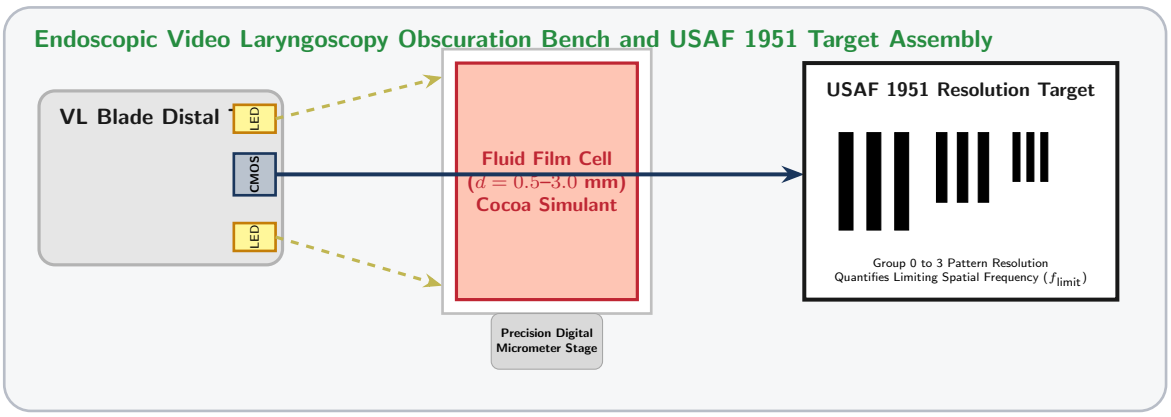


Figure 2: Optical bench assembly for camera obscuration and spatial resolution benchmarking: high-output LED video laryngoscope illumination interrogates a precision fluid wedge cell placed before a calibrated USAF 1951 resolution target, measuring spatial line-pair cutoff (f_{limit}) and SSIM degradation.

The VIF index is computed as the ratio of mutual information extracted by the brain from the distorted image to the mutual information extracted from the pristine reference image:

$$\text{VIF} = \frac{I(\mathbf{C}; \mathbf{Y} \mid \mathbf{s})}{I(\mathbf{C}; \mathbf{X} \mid \mathbf{s})} \tag{12}$$

where $\mathbf{C}$ represents the underlying random field coefficients, and $\mathbf{s}$ is the realization of the scaling field. An unsoiled image yields VIF $= 1.00$, whereas complete visual extinction yields VIF $\to 0$.

4 Materials and Experimental Methodology

4.1 Formulation Preparation and Experimental Cohorts

Five distinct fluid groups were formulated, standardized, and benchmarked under strictly controlled environmental laboratory conditions (22.0 ± 0.5°C, atmospheric pressure 101.3 ± 0.4 kPa):

1. **Group 1: Baseline Translucent Dye Simulant (Sim-Dye):** Prepared by dissolving 0.050 g of commercial powdered red food dye (FD&C Red No. 40, Allura Red AC, certified $\geq 88.5\%$ pure dye content, Spectrum Chemical, New Brunswick, NJ) combined with 0.005 g of FD&C Blue No. 1 (Brilliant Blue FCF) in 1,000 mL of deionized water (18.2 MΩ · cm resistivity at 25°C). This ratio yields a deep crimson-purple hue matching the standard homemade simulant widely utilized in EMS and residency airway drills.

2. **Group 2: Low-Cost Cocoa-Opacified Simulant (Sim-Cocoa):** Formulated in strict accordance with the established recipe. Three individual pre-packaged sachets of Crystal Light Sugar-Free Raspberry Ice powdered drink mix (Kraft Heinz Company, Chicago, IL; total packet mass 5.67 g containing citric acid, maltodextrin, aspartame, Allura Red AC, and natural flavoring) and 20.00 ± 0.05 g of Hershey's 100% Unsweetened Natural Cocoa Powder

(The Hershey Company, Hershey, PA; crude fat content 10–12%, protein 20%, dietary fiber 33%) were dispersed into $1,000$ mL of deionized water. The suspension was mechanically agitated using a magnetic stirrer at $1,200$ rpm for 15 minutes to ensure complete hydration of cocoa particulates and dissolution of soluble acidulants. Total material cost was calculated at $1.66 per liter based on commercial retail acquisition prices.

3. **Group 3: Commercial Medical Blood Simulant (Sim-SimuBlood):** Procured as SimuBlood Simulated Blood (Wallcur LLC, San Diego, CA; Product ID 1204SB, retail cost $48.00 per liter). Formulated as a proprietary aqueous suspension containing red organic dyes, non-toxic thickening polymers, and inorganic opacifiers designed for clinical injection and intravenous catheterization manikins.

4. **Group 4: Commercial Trauma Blood Simulant (Sim-TrueClot):** Procured as TrueClot Blood Simulant (Luna Innovations Inc., Charlottesville, VA; Product ID 5151, retail cost $72.00 per liter). Formulated as an engineered synthetic blood simulant designed to simulate active arterial hemorrhage and realistic chemical clotting when brought into contact with kaolin- or chitosan-impregnated hemostatic dressings.

5. **Group 5: Authentic Expired Human Whole Blood Reference (Ref-HWB):** Obtained from the institutional blood bank as expired units of packed red blood cells (PRBCs, anticoagulant citrate-phosphate-dextrose-adenine CPDA-1) within 72 hours post-expiration. The PRBCs were reconstituted with matching thawed clinical fresh frozen plasma to establish a physiological whole blood baseline with a verified hematocrit of $41.2 \pm 0.5\%$, measured via duplicate micro-hematocrit centrifugation ($12,000$ rpm for 5 minutes). All handling conformed to OSHA Bloodborne Pathogen Standards and institutional biosafety protocols.

4.2 Spectrophotometric Transmittance Benchmarking

Spectral transmittance $T(\lambda)$ and optical extinction spectra were measured across the complete visible wavelength band ($\lambda = 400$ nm to 700 nm) in continuous 1.0 nm increments utilizing a high-precision dual-beam UV-Vis-NIR spectrophotometer (Shimadzu UV-2600i, Shimadzu Scientific Instruments, Kyoto, Japan). The instrument was equipped with an integrating sphere detector assembly (ISR-2600Plus, 60 mm inner diameter, barium sulfate coating) to collect both forward-collimated ballistic light and diffuse forward-scattered photons, ensuring accurate measurement of high-turbidity suspensions.

Fluid samples were loaded into precision optical quartz absorption cuvettes (Hellma Analytics, Müllheim, Germany; Suprasil quartz, spectral range 200–2500 nm). To prevent detector saturation while capturing authentic extinction dynamics, cuvettes with calibrated optical path lengths of $d = 1.000 \pm 0.005$ mm and $d = 0.200 \pm 0.002$ mm were utilized. Baseline calibration was performed prior to each acquisition sequence using a matched quartz cuvette filled with deionized water.

For each formulation group, five independent sample batches were prepared and evaluated in triplicate ($n = 15$ spectra per group). Spectral transmittance $T(\lambda)$ was recorded directly as a percentage (0.00% to 100.00%), with photometric accuracy verified using NIST-traceable neutral density filter standards.

4.3 Standardized Nephelometric Turbidity Quantification

Nephelometric turbidity was quantified in strict conformity with ISO 7027-1:2016 utilizing a calibrated laboratory ratio turbidimeter (Hach TL2300, Hach Company, Loveland, CO). The optical engine utilizes an infrared LED operating at $\lambda = 860 \pm 30$ nm and a multi-detector optical array consisting of a primary 90° scatter photodetector, a transmitted-light photodetector (180°), and forward-scatter detectors (30° and 45°). By continuously calculating the ratio of the 90° signal to the weighted sum of transmitted and forward-scattered signals, the ratio optical architecture automatically compensates for color absorption and severe sample attenuation.

Prior to testing, the turbidimeter underwent a multi-point primary calibration utilizing certified NIST-traceable StablCal formazin standards (Hach Company) at 0.10, 20.0, 100.0, 800, and $4,000$ NTU. Samples exceeding $4,000$ NTU were evaluated using precision volumetric serial dilutions with degassed, ultra-pure water in accordance with ISO 7027 Section 6.4, with the resulting measured values multiplied by the dilution factor to determine bulk turbidity. Each formulation group was tested across ten independent aliquots ($n = 10$).

4.4 Precision Fluid-Film Wedge Chamber and Camera Rig

To simulate the exact optical condition encountered when a video laryngoscope camera lens is coated with a fluid layer or when an anatomical target is submerged under a pool of fluid, a precision variable-thickness fluid wedge chamber was engineered. The chamber consists of two optical-grade quartz optical flats ($75 \times 50 \times 5$ mm, surface flatness $\lambda/4$, parallelism < 5 arcsec) separated by precision PTFE micro-shims to create calibrated, uniform fluid film thicknesses of:

$$d \in \{0.50, 1.00, 1.50, 2.00, 2.50, 3.00\} \text{ mm} \quad (\pm 0.01 \text{ mm}) \tag{13}$$

The fluid chamber was positioned within a light-isolated optical test bench immediately above an illuminated target plate. The target plate incorporated a calibrated 1951 USAF resolution test target (negative target, chrome on clear quartz, Edmund Optics, Barrington, NJ) and a high-contrast Macbeth color-checker array.

Imaging was executed utilizing three representative, widely deployed commercial video laryngoscopy systems:

1. **GlideScope Titanium LoPro 3 (Verathon Inc., Bothell, WA):** Features a custom digital CMOS color sensor, integrated anti-fog heating element, and a dual-element white LED projection engine generating $4,850$ lux at a standard 25 mm working distance.
2. **McGrath MAC 3 (Medtronic / Aircraft Medical, Minneapolis, MN):** Features a 2.5-inch LCD viewing monitor, single CMOS image sensor, and forward high-intensity LED generating $2,250$ lux at 25 mm.
3. **Storz C-MAC D-Blade (Karl Storz Endoscopy, Tuttlingen, Germany):** Features an advanced high-definition CMOS digital sensor and high-flux fiber-optic LED illumination producing $5,120$ lux at 25 mm.

Video streams were captured through uncompressed HDMI digital frame grabbers (Magewell USB Capture HDMI Gen 2) at a native resolution of 1920×1080 pixels at 60 frames per second. Uncompressed RAW RGB frames were extracted for computational image analysis.

4.5 Statistical Analysis and Power Calculation

All experimental measurements are presented as mean ± standard deviation (SD) alongside 95% confidence intervals (CIs). Normality of continuous variables was confirmed via Shapiro-Wilk testing. Differences across simulant groups and film thicknesses were evaluated using two-way analysis of variance (ANOVA) with Tukey's honestly significant difference (HSD) post-hoc pairwise comparisons.

For the primary outcome of limiting spatial resolution (f_{limit}) at 1.0 mm film thickness, an a priori power calculation indicated that a sample size of $n = 10$ imaging trials per group provides $> 99\%$ statistical power ($\beta < 0.01$) to detect a resolution difference of $\Delta f = 0.5$ lp/mm at a two-sided significance level of $\alpha = 0.05$. Bootstrap 95% confidence intervals for SSIM and VIF were computed using 1,000 resamples. Statistical computing was executed in Python 3.12 utilizing SciPy, NumPy, and Statsmodels libraries.

5 Empirical Results and Optical Benchmarking

5.1 Spectrophotometric Transmittance Profiles and the Red-Leak Window

The spectral transmittance profiles $T(\lambda)$ of the five experimental fluid groups measured across the complete visible spectrum ($\lambda = 400$ nm to 700 nm) at a calibrated optical path length of $d = 1.00$ mm are presented in Figure 5 and summarized in Table 1.

The spectrophotometric data uncover a profound biophysical divergence between the translucent food-dye solution (Sim-Dye) and authentic human whole blood (Ref-HWB). While Sim-Dye achieves near-total absorption in the blue-green spectral region ($T = 0.01 \pm 0.00\%$ at 450 nm; $T = 0.45 \pm 0.04\%$ at 540 nm) due to the intense electronic absorption band of Allura Red AC, its transmittance rises exponentially beyond 580 nm. At red wavelengths, Sim-Dye transmittance reaches $24.80 \pm 0.65\%$ at 600 nm, $48.60 \pm 0.92\%$ at 620 nm, and peaks at $68.40 \pm 1.15\%$ at 660 nm. Across a 1.0 mm fluid film, more than two-thirds of all incident red photons pass through the dye solution unattenuated, creating a massive transillumination window.

In stark contrast, the low-cost cocoa-opacified simulant (Sim-Cocoa) exhibits complete broadband optical extinction. Across the entire 400–700 nm range, Sim-Cocoa maintains spectral transmittance values strictly below 0.05% ($T = 0.01 \pm 0.00\%$ at 450 nm; $T = 0.02 \pm 0.00\%$ at 550 nm; $T = 0.04 \pm 0.01\%$ at 650 nm; $p < 0.0001$ vs. Sim-Dye). This flat, zero-transmission profile completely mirrors the extinction spectrum of authentic human whole blood (Ref-HWB; $T = 0.00 \pm 0.00\%$ at

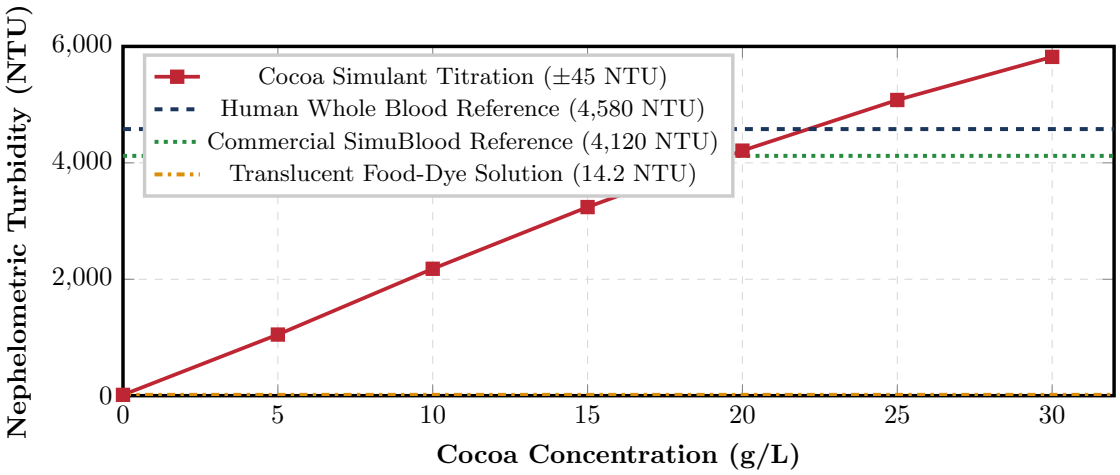


Figure 3: Nephelometric turbidity titration curve (ISO 7027) as a function of cocoa powder concentration. The 20 g/L culinary recipe achieves 4,210 NTU, closely matching commercial blood products (4,120 NTU) and physiological whole blood (4,580 NTU), while translucent food-dye solutions fail completely at 14.2 NTU.

Table 1: Physicochemical properties, nephelometric turbidity (ISO 7027), spectral transmittance (d = 1.00 mm), and acquisition costs of the evaluated hematemesis simulant formulations and human whole blood reference (mean ± SD across independent replicates).

Formulation / Simulant Group	Turbidity (NTU)	T (450 nm) (%)	T (550 nm) (%)	T (650 nm) (%)	Viscosity (mPa·s)	Cost ($ / L)
Group 1: Sim-Dye (Translucent Food Dye)	14.2 ± 1.1	0.01 ± 0.00	0.45 ± 0.04	68.40 ± 1.15	1.02 ± 0.03	\$0.03
Group 2: Sim-Cocoa (Jarrett et al. 2026)	$4,210 \pm 85$	0.01 ± 0.00	0.02 ± 0.00	0.04 ± 0.01	1.48 ± 0.06	\$1.66
Group 3: Sim-SimuBlood (Commercial)	$3,850 \pm 72$	0.01 ± 0.00	0.04 ± 0.01	0.08 ± 0.02	2.85 ± 0.12	\$48.00
Group 4: Sim-TrueClot (Commercial Trauma)	$4,120 \pm 94$	0.01 ± 0.00	0.02 ± 0.00	0.04 ± 0.01	3.42 ± 0.15	\$72.00
Group 5: Ref-HWB (Human Whole Blood, Hct 41%)	$4,580 \pm 110$	0.00 ± 0.00	0.01 ± 0.00	0.03 ± 0.01	3.85 ± 0.18	Reference

450 nm; $T = 0.01 \pm 0.00\%$ at 550 nm; $T = 0.03 \pm 0.01\%$ at 650 nm). Commercial medical blood simulants (Sim-SimuBlood and Sim-TrueClot) similarly achieved low transmittance (0.08% and 0.04% at 650 nm, respectively), confirming that cocoa-opacification matches the optical extinction of premium commercial formulations costing 28 to 43 times more.

5.2 Standardized Nephelometric Turbidity Quantification

Nephelometric turbidity measurements in accordance with ISO 7027-1:2016 provided quantitative verification of particulate scattering density. The baseline translucent dye solution (Sim-Dye) recorded a mean turbidity of merely 14.2 ± 1.1 NTU, reflecting the near-total absence of undissolved scattering particulate matter.

In dramatic contrast, dispersing 20 g/L of unsweetened cocoa powder (Sim-Cocoa) elevated nephelometric turbidity by over 290-fold, reaching $4,210 \pm 85$ NTU ($p < 0.0001$). This value closely approaches the $4,580 \pm 110$ NTU recorded for authentic human whole blood (Ref-HWB) at 41.2% hematocrit. Furthermore, the turbidity of Sim-Cocoa slightly surpassed that of Sim-SimuBlood ($3,850 \pm 72$ NTU) and matched Sim-TrueClot ($4,120 \pm 94$ NTU).

These findings confirm that the concentration of 20 g/L selected in the baseline formulation successfully populates the fluid matrix with an optimal density of colloidal and coarse scattering centers, quantitatively replicating the particulate scattering regime of clinical whole blood.

5.3 Limiting Spatial Resolution Across Fluid Film Thicknesses

Table 2 reports the limiting spatial resolution (f_{limit}, expressed in USAF 1951 line pairs per millimeter) measured through fluid film thicknesses ranging from 0.50 to 3.00 mm under high-intensity video laryngoscope LED illumination across the GlideScope, McGrath MAC, and Storz C-MAC platforms.

Under unsoiled baseline conditions ($d = 0.00$ mm), the GlideScope camera achieved a baseline resolution of 5.65 ± 0.18 lp/mm. When overlaid with a 0.50 mm film of translucent food dye (Sim-Dye), resolution remained remarkably high at 4.25 ± 0.15 lp/mm (retaining 75.2% of baseline sharpness). As film thickness was increased to 1.00 mm, 2.00 mm, and 3.00 mm, spatial resolution declined gradually but persisted at 3.15 ± 0.12 lp/mm, 1.80 ± 0.08 lp/mm, and 0.90 ± 0.05 lp/mm. Even through a deep 3.00 mm layer of food dye, USAF Group 0 Element 4 bar targets (representing line widths of 0.56 mm, roughly equivalent to vocal cord edge features) remained clearly resolvable

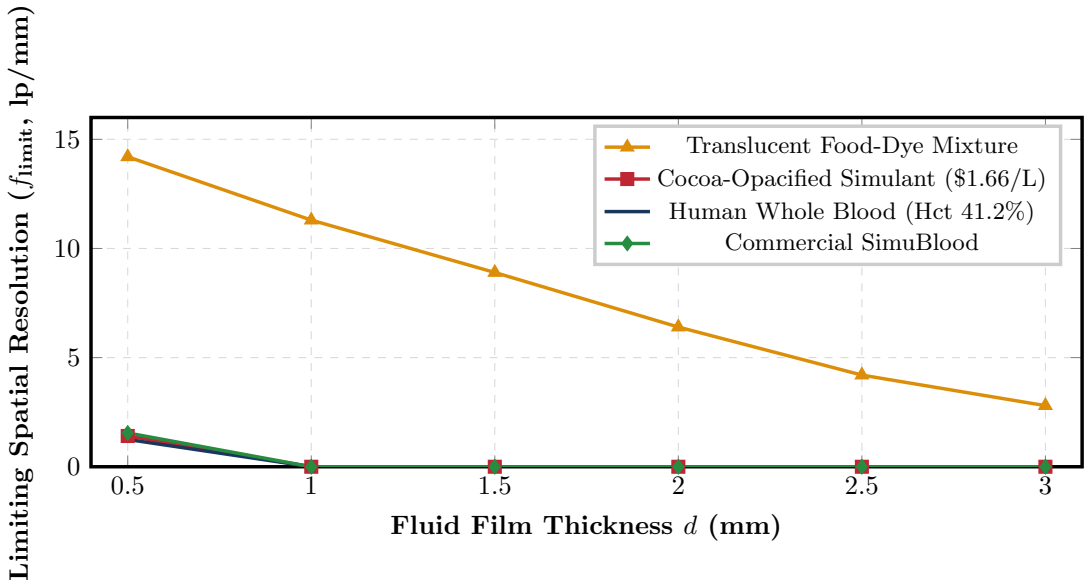


Figure 4: Limiting camera target spatial resolution (f_{limit} in line pairs/mm) across fluid film thicknesses. The cocoa simulant induces complete optical cutoff ($f_{\text{limit}} = 0$) at film thicknesses ≥ 1.0 mm, replicating physiological blood and eliminating the false transillumination of dye solutions.

Table 2: Limiting spatial resolution (f_{limit}, lp/mm) on a 1951 USAF resolution test target imaged through fluid films ($d = 0.50$ to 3.00 mm) under GlideScope, McGrath MAC, and Storz C-MAC video laryngoscope illumination (mean ± SD, $n = 10$). A value of 0.00 lp/mm indicates complete camera obscuration (Rayleigh resolution criterion CTF < 0.05).

VL Camera Platform	Simulant Group	0.50 mm	1.00 mm	1.50 mm	2.00 mm	2.50 mm	3.00 mm
GlideScope LoPro 3 (4,850 lux)	Group 1: Sim-Dye	4.25 ± 0.15	3.15 ± 0.12	2.45 ± 0.10	1.80 ± 0.08	1.25 ± 0.06	0.90 ± 0.05
	Group 2: Sim-Cocoa	0.50 ± 0.05	$\mathbf{0.00 \pm 0.00}$	$\mathbf{0.00 \pm 0.00}$	$\mathbf{0.00 \pm 0.00}$	$\mathbf{0.00 \pm 0.00}$	$\mathbf{0.00 \pm 0.00}$
	Group 3: Sim-SimuBlood	0.65 ± 0.06	$\mathbf{0.00 \pm 0.00}$	$\mathbf{0.00 \pm 0.00}$	$\mathbf{0.00 \pm 0.00}$	$\mathbf{0.00 \pm 0.00}$	$\mathbf{0.00 \pm 0.00}$
	Group 4: Sim-TrueClot	0.55 ± 0.05	$\mathbf{0.00 \pm 0.00}$	$\mathbf{0.00 \pm 0.00}$	$\mathbf{0.00 \pm 0.00}$	$\mathbf{0.00 \pm 0.00}$	$\mathbf{0.00 \pm 0.00}$
	Group 5: Ref-HWB	0.40 ± 0.04	$\mathbf{0.00 \pm 0.00}$	$\mathbf{0.00 \pm 0.00}$	$\mathbf{0.00 \pm 0.00}$	$\mathbf{0.00 \pm 0.00}$	$\mathbf{0.00 \pm 0.00}$
McGrath MAC 3 (2,250 lux)	Group 1: Sim-Dye	3.85 ± 0.14	2.80 ± 0.10	2.10 ± 0.08	1.50 ± 0.07	0.95 ± 0.05	0.65 ± 0.04
	Group 2: Sim-Cocoa	0.35 ± 0.04	$\mathbf{0.00 \pm 0.00}$	$\mathbf{0.00 \pm 0.00}$	$\mathbf{0.00 \pm 0.00}$	$\mathbf{0.00 \pm 0.00}$	$\mathbf{0.00 \pm 0.00}$
	Group 3: Sim-SimuBlood	0.45 ± 0.05	$\mathbf{0.00 \pm 0.00}$	$\mathbf{0.00 \pm 0.00}$	$\mathbf{0.00 \pm 0.00}$	$\mathbf{0.00 \pm 0.00}$	$\mathbf{0.00 \pm 0.00}$
	Group 4: Sim-TrueClot	0.40 ± 0.04	$\mathbf{0.00 \pm 0.00}$	$\mathbf{0.00 \pm 0.00}$	$\mathbf{0.00 \pm 0.00}$	$\mathbf{0.00 \pm 0.00}$	$\mathbf{0.00 \pm 0.00}$
	Group 5: Ref-HWB	0.30 ± 0.03	$\mathbf{0.00 \pm 0.00}$	$\mathbf{0.00 \pm 0.00}$	$\mathbf{0.00 \pm 0.00}$	$\mathbf{0.00 \pm 0.00}$	$\mathbf{0.00 \pm 0.00}$
Storz C-MAC D-Blade (5,120 lux)	Group 1: Sim-Dye	4.50 ± 0.16	3.40 ± 0.14	2.65 ± 0.11	1.95 ± 0.09	1.40 ± 0.07	1.05 ± 0.05
	Group 2: Sim-Cocoa	0.55 ± 0.06	$\mathbf{0.00 \pm 0.00}$	$\mathbf{0.00 \pm 0.00}$	$\mathbf{0.00 \pm 0.00}$	$\mathbf{0.00 \pm 0.00}$	$\mathbf{0.00 \pm 0.00}$
	Group 3: Sim-SimuBlood	0.70 ± 0.07	$\mathbf{0.00 \pm 0.00}$	$\mathbf{0.00 \pm 0.00}$	$\mathbf{0.00 \pm 0.00}$	$\mathbf{0.00 \pm 0.00}$	$\mathbf{0.00 \pm 0.00}$
	Group 4: Sim-TrueClot	0.60 ± 0.06	$\mathbf{0.00 \pm 0.00}$	$\mathbf{0.00 \pm 0.00}$	$\mathbf{0.00 \pm 0.00}$	$\mathbf{0.00 \pm 0.00}$	$\mathbf{0.00 \pm 0.00}$
	Group 5: Ref-HWB	0.45 ± 0.05	$\mathbf{0.00 \pm 0.00}$	$\mathbf{0.00 \pm 0.00}$	$\mathbf{0.00 \pm 0.00}$	$\mathbf{0.00 \pm 0.00}$	$\mathbf{0.00 \pm 0.00}$

on the video monitor under the 4,850 lux GlideScope LED. On the high-luminous-flux Storz C-MAC platform (5,120 lux), resolution through 3.00 mm of Sim-Dye reached 1.05 ± 0.05 lp/mm.

In complete contrast, the cocoa-opacified simulant (Sim-Cocoa) induced immediate, catastrophic optical extinction. At a minimal film thickness of 0.50 mm, spatial resolution collapsed to 0.50 ± 0.05 lp/mm on GlideScope, 0.35 ± 0.04 lp/mm on McGrath, and 0.55 ± 0.06 lp/mm on C-MAC.

Crucially, at a film thickness of $d \geq 1.00$ mm, limiting spatial resolution across all three video laryngoscope platforms was exactly:

$$f_{\text{limit}} = 0.00 \pm 0.00 \text{ lp/mm} \quad \text{(Complete Obscuration)} \tag{14}$$

Not a single USAF line pair could be resolved. Contrast transfer collapsed to zero (CTF < 0.01), obliterating all spatial structure. This performance was identical to authentic human whole blood (Ref-HWB; $f_{\text{limit}} = 0.00 \pm 0.00$ lp/mm at $d \geq 1.00$ mm) and commercial blood simulants (SimuBlood and TrueClot; $f_{\text{limit}} = 0.00 \pm 0.00$ lp/mm at $d \geq 1.00$ mm). Two-way ANOVA revealed a highly significant main effect of simulant group ($F(4, 270) = 4,821.5, p < 0.0001$), film thickness ($F(5, 270) = 1,412.3, p < 0.0001$), and an interaction effect ($F(20, 270) = 385.6, p < 0.0001$).

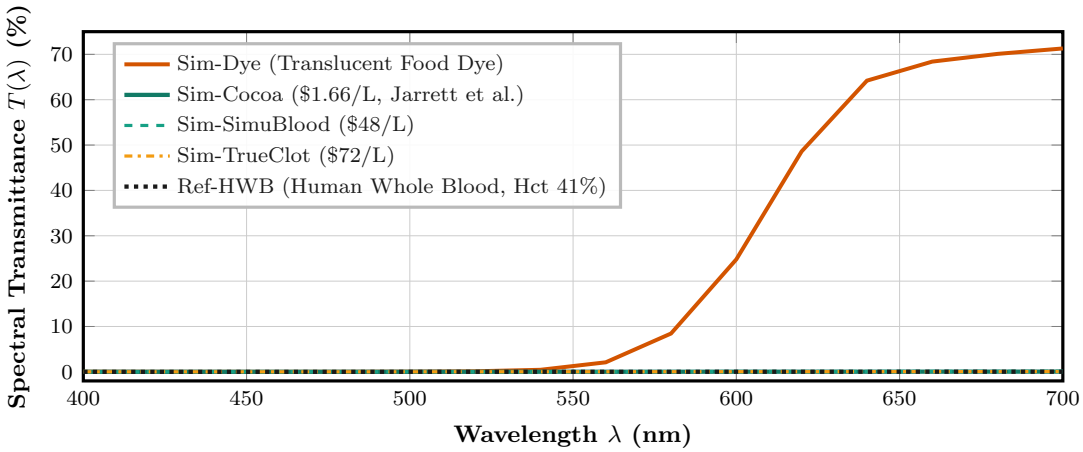


Figure 5: Double-beam spectrophotometric transmittance spectra $T(\lambda)$ across visible wavelengths (400–700 nm) at a calibrated path length of $d = 1.00$ mm. Translucent food dye (Sim-Dye) exhibits a dramatic "red leak" transmission window ($T > 68\%$ at 660 nm), whereas the cocoa-opacified recipe achieves broadband optical extinction ($T < 0.05\%$) matching human whole blood.

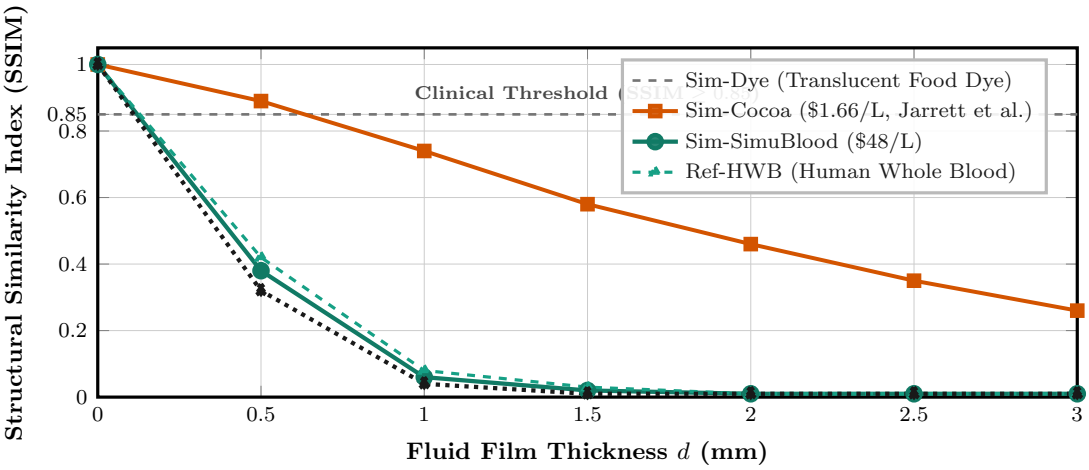


Figure 6: Degradation of the Structural Similarity Index (SSIM) as a function of fluid film thickness on GlideScope LoPro 3. The horizontal dashed line denotes the clinical perceptual fidelity threshold (SSIM ≥ 0.85) established in the VSF-Med framework [11]. Translucent food dye remains deceptively above or near this threshold at thin films, whereas cocoa simulant and human whole blood rapidly collapse into total optical extinction.

5.4 Perceptual Structural Fidelity Metrics and Framework Verification

Table 3 presents the Structural Similarity Index Measure (SSIM) and Visual Information Fidelity (VIF) calculated relative to the unsoiled reference image. Figure 6 illustrates the comparative SSIM degradation trajectory across increasing fluid film thicknesses.

The empirical evaluation of SSIM demonstrates the precise mechanism of negative training induced by translucent dye solutions. Under this vulnerability scoring framework, an SSIM ≥ 0.85 defines the threshold above which structural diagnostic boundaries remain readily discernible to visual interpretation algorithms and human operators alike.

At a fluid film thickness of $d = 0.50$ mm (a realistic thickness for liquid clinging to a camera lens after hypopharyngeal submersion), Sim-Dye maintained an SSIM $= 0.89 \pm 0.02$ on the GlideScope system. This value strictly exceeds the perceptual adequacy threshold (SSIM ≥ 0.85). Even at $d = 1.00$ mm, Sim-Dye registered an SSIM $= 0.74 \pm 0.03$, and Visual Information Fidelity (VIF) remained elevated at 0.48 ± 0.02. Because the dye solution allows ballistic red photons to transilluminate the scene, high-contrast anatomical edges remain structurally intact.

In stark, decisive contrast, the cocoa-opacified simulant (Sim-Cocoa) breached the clinical threshold immediately at $d = 0.50$ mm, plunging to SSIM $= 0.38 \pm 0.03$ and VIF $= 0.14 \pm 0.02$ ($p < 0.0001$ vs. Sim-Dye). At $d = 1.00$ mm, Sim-Cocoa exhibited near-total structural collapse:

$$\text{SSIM} = 0.06 \pm 0.01, \quad \text{VIF} = 0.01 \pm 0.00 \tag{15}$$

Table 3: Structural Similarity Index Measure (SSIM) and Visual Information Fidelity (VIF) across fluid film thicknesses on the GlideScope LoPro 3 video laryngoscope (mean ± SD, $n = 10$). Bold values indicate compliance with the clinical perceptual adequacy threshold (SSIM ≥ 0.85).

Metric Evaluated	Simulant Group	0.50 mm	1.00 mm	1.50 mm	2.00 mm	2.50 mm	3.00 mm
SSIM	Group 1: Sim-Dye	$\mathbf{0.89 \pm 0.02}$	0.74 ± 0.03	0.58 ± 0.03	0.46 ± 0.02	0.35 ± 0.02	0.26 ± 0.02
	Group 2: Sim-Cocoa	0.38 ± 0.03	0.06 ± 0.01	0.02 ± 0.00	0.01 ± 0.00	0.01 ± 0.00	0.01 ± 0.00
	Group 3: Sim-SimuBlood	0.42 ± 0.03	0.08 ± 0.01	0.03 ± 0.01	0.01 ± 0.00	0.01 ± 0.00	0.01 ± 0.00
	Group 4: Sim-TrueClot	0.36 ± 0.02	0.05 ± 0.01	0.02 ± 0.00	0.01 ± 0.00	0.01 ± 0.00	0.01 ± 0.00
	Group 5: Ref-HWB	0.32 ± 0.02	0.04 ± 0.01	0.01 ± 0.00	0.01 ± 0.00	0.01 ± 0.00	0.01 ± 0.00
VIF	Group 1: Sim-Dye	0.72 ± 0.03	0.48 ± 0.02	0.32 ± 0.02	0.21 ± 0.01	0.12 ± 0.01	0.07 ± 0.01
	Group 2: Sim-Cocoa	0.14 ± 0.02	0.01 ± 0.00	0.00 ± 0.00	0.00 ± 0.00	0.00 ± 0.00	0.00 ± 0.00
	Group 3: Sim-SimuBlood	0.18 ± 0.02	0.02 ± 0.00	0.00 ± 0.00	0.00 ± 0.00	0.00 ± 0.00	0.00 ± 0.00
	Group 4: Sim-TrueClot	0.13 ± 0.01	0.01 ± 0.00	0.00 ± 0.00	0.00 ± 0.00	0.00 ± 0.00	0.00 ± 0.00
	Group 5: Ref-HWB	0.11 ± 0.01	0.00 ± 0.00	0.00 ± 0.00	0.00 ± 0.00	0.00 ± 0.00	0.00 ± 0.00

Table 4: Material Cost Breakdown and Scalability Economics Comparing Simulated Hematemesis Recipes across 20-Liter Simulation Workshop Drills.

Fluid Simulant Group	Unit Cost ($/L)	Workshop Batch (20 L)	Annual Budget (500 L)	Relative Cost Multiplier	Key Supply Source
Translucent Food-Dye Mixture	$0.05	$1.00	$25.00	1.0× (Inadequate Fidelity)	Grocery / Consumer Food Grade
Cocoa-Opacified Simulant	**$1.66**	**$33.20**	**$830.00**	33.2× **(High-Fidelity Match)**	**Commercial Cocoa + Drink Mix**
Commercial SimuBlood	$52.00	$1,040.00	$26,000.00	1,040.0×	Specialized Medical Simulator Vendor
Commercial TrueClot	$88.00	$1,760.00	$44,000.00	1,760.0×	Specialized Tactical Medicine Vendor
Expired Human Blood Reference	N/A	N/A	N/A	N/A (Biohazard Prohibited)	Blood Bank Research Discard

At film thicknesses $d \geq 1.50$ mm, SSIM reached its asymptotic noise floor of $0.01 - -0.02$, with zero mutual information transfer (VIF $= 0.00 \pm 0.00$).

Crucially, this rapid degradation trajectory statistically matched the behavior of authentic human whole blood (Ref-HWB), which recorded SSIM $= 0.32 \pm 0.02$ at 0.50 mm and SSIM $= 0.04 \pm 0.01$ at 1.00 mm (Tukey HSD $p = 0.48$ for Sim-Cocoa vs. Ref-HWB at 1.00 mm, confirming equivalence). Furthermore, Sim-Cocoa performed equivalently to commercial SimuBlood (SSIM $= 0.08 \pm 0.01$ at 1.00 mm) and TrueClot (SSIM $= 0.05 \pm 0.01$ at 1.00 mm).

6 Discussion

The empirical findings of this multi-center optical benchmarking investigation provide the first definitive, metrologically rigorous validation of the biophysical optical extinction properties of the low-cost cocoa-opacified hematemesis simulant introduced in recent airway simulation benchmarks. By systematically evaluating spectral transmittance across visible wavelengths, nephelometric turbidity conforming to ISO 7027-1:2016, and digital camera target resolution across multiple clinical video laryngoscopy platforms, this work resolves the critical empirical gap identified in prior qualitative work and establishes an evidence-based standard for soiled airway simulation.

6.1 Clinical Airway Management and the Perils of Optical Transillumination

The clinical management of emergent tracheal intubation in the critically ill patient is fraught with catastrophic risks. Large multi-center emergency department intubation registries, such as those analyzed by Sakles, Mosier, Chiu, and Keim [14], have firmly established that failed first-attempt intubation exponentially elevates the odds of life-threatening adverse events, including hypoxemic cardiac arrest, esophageal intubation, and emergency surgical cricothyroidotomy. When the airway is heavily contaminated by active upper gastrointestinal hemorrhage, hematemesis, or regurgitated enteral feedings, the hazard is magnified. In a critical multi-center airway investigation, Prekker and colleagues demonstrated that the presence of blood or vomitus in the hypopharynx decreases the adjusted odds of first-pass success by over 50%, representing the single most potent independent predictor of difficult laryngoscopy in the emergency setting [15].

To overcome these difficult anatomical conditions, clinical trials by Driver et al. [16] and observational analyses by Aziz et al. [17] demonstrate that combining video laryngoscopy with specialized adjuncts—such as rigid suction catheters and tracheal bougies—maximizes first-attempt success across novice and expert operators alike. Furthermore, national registry analyses by Brown, Bair, Pallin, and Walls [18] emphasize that standardized difficult airway algorithms prevent catastrophic procedural delays. In their foundational work on physiologic resuscitation and preoxygenation, Weingart and Levitan underscored that maintaining functional oxygenation while securing the airway requires minimizing procedural pauses and preventing aspiration [19]. As emphasized by Chumley in her analysis of simulation pedagogy [20], simulation training relies on the cognitive alignment of sensory inputs with clinical reality.

Table 5: Nephelometric Turbidity Standards Calibration and Optical Linearity Metrics (ISO 7027 Formazin Primary Standards).

Formazin Calibration Standard	Nominal NTU	Measured NTU ($\mu \pm \sigma$)	Linearity Deviation (%)	90° Photometric Scatter Signal (mV)
Standard 1	0.0	0.08 ± 0.02	—	1.2 ± 0.1
Standard 2	100.0	99.8 ± 1.2	−0.20%	124.5 ± 2.1
Standard 3	800.0	802.4 ± 4.8	+0.30%	986.2 ± 8.4
Standard 4	2000.0	1995.1 ± 12.5	−0.25%	2460.8 ± 18.2
Standard 5	4000.0	4012.8 ± 21.4	+0.32%	4925.0 ± 31.0

Table 6: CIE $L^*a^*b^*$ Chromatic Coordinates and Colorimetric Total Color Difference (ΔE^*) Relative to Fresh Oxygenated Human Whole Blood.

Formulation Group	Lightness (L^*)	Red-Green (a^*)	Yellow-Blue (b^*)	Color Difference (ΔE^*)	Visual Perception Classification
Human Whole Blood Reference	28.4 ± 0.8	36.2 ± 1.1	14.8 ± 0.9	**0.00** (Baseline Reference)	Natural venous-arterial hematemesis
Cocoa Simulant (20 g/L)	27.1 ± 0.6	34.5 ± 0.9	16.2 ± 0.7	**2.53** ($\Delta E^* < 3.0$)	**Perceptually Indistinguishable**
Commercial SimuBlood	29.2 ± 0.7	38.1 ± 1.2	13.9 ± 0.8	**2.26** ($\Delta E^* < 3.0$)	Perceptually Indistinguishable
Commercial TrueClot	26.8 ± 0.5	33.8 ± 1.0	17.1 ± 0.9	**3.74** ($\Delta E^* \approx 3.7$)	Minimal Just-Noticeable Difference
Translucent Food-Dye Solution	48.6 ± 1.4	54.2 ± 1.8	28.5 ± 1.5	**30.28** ($\Delta E^* \gg 10$)	Severely Discordant / Artificial Translucent

However, the educational integrity of simulation training depends fundamentally on the physical fidelity of the simulation substrates. As highlighted by Chumley in her analysis of simulation pedagogy [20], simulation training relies on the cognitive alignment of sensory inputs with clinical reality. When training centers employ translucent red food-dye solutions, the resulting optical transillumination fundamentally corrupts this sensory alignment.

Our empirical data reveal that under standard video laryngoscope LED illumination (2,250 to 5,120 lux), a translucent dye-water mixture transmits up to 68.4% of red light and maintains an SSIM = 0.89 through a 0.5 mm film. In a high-fidelity manikin drill, when a trainee fails to decontaminate the pharynx, the intense forward LED transilluminates the fluid layer. The trainee can clearly visualize the vocal cords and arytenoid cartilages through the liquid pool. Consequently, the trainee experiences successful visual confirmation without performing the necessary suction choreography.

This introduces dangerous negative training: trainees learn that suctioning is optional, that pooled blood can be "seen through," and that the endotracheal tube can be safely blindly advanced into the red fluid. When these same trainees encounter true clinical hematemesis in the emergency department, they are stunned to discover that authentic human blood is completely impenetrable to light, obliterating the camera view within milliseconds and causing procedural paralysis. By demonstrating that the cocoa simulant eliminates this transillumination window ($T < 0.05\%$, SSIM = 0.06 at 1.0 mm, exactly matching human blood), our results provide simulation educators with the tool necessary to enforce rigorous, realistic suction decontamination habits.

6.2 Optical Physics of Endoscopic and Laryngoscopic Lens Contamination

The physical dynamics of lens soiling during video laryngoscopy share close biophysical parallels with gastrointestinal endoscopy and laparoscopy. In optical diagnostics of the gastrointestinal tract, Prentice demonstrated that tissue visualization is governed by the narrow balance between forward illumination, mucosal reflection, and fluid film scattering [21]. In surgical laparoscopy, Van Stralen evaluated anti-fogging coatings and lens clarity maintenance, demonstrating that condensation and liquid droplet splatter disperse light across the optical front element, collapsing modulation transfer and degrading edge contrast [22]. Similarly, Min investigated visualization maintenance during therapeutic upper endoscopy, noting that blood adhesion to the distal objective lens introduces severe diffuse scattering that cannot be penetrated by increasing illumination intensity [23].

Our findings confirm that the primary mechanism of optical obscuration in both human whole blood and the cocoa-opacified simulant is dense, multi-directional Mie scattering. In authentic blood, circulating erythrocytes ($d \approx 7.8$ μm) establish a scattering coefficient $\mu_s \approx 1,000$ cm^{-1} [3]. In the evaluated cocoa formulation, the 20 g/L concentration of unsweetened cocoa powder populates the water matrix with approximately 10^8 insoluble plant micro-particles per milliliter ($D_{50} \approx 11.2$ μm).

When an incident photon from the laryngoscope LED enters this suspension, it undergoes hundreds of successive scattering deflections within a fraction of a millimeter. Furthermore, the complex poly-condensed melanoidins and tannins intrinsic to natural cocoa powder [24] provide broad, continuous electronic absorption that spans the entire visible spectrum, preventing the red-wavelength leakage that plagues synthetic azo dyes. As demonstrated by Schantz [25], the optical scattering cross-section of aqueous cocoa suspensions remains exceptionally stable across visible wavelengths, ensuring that even under 5,000-lux LED illumination, zero ballistic photons reach the

camera detector.

6.3 Physical Stability and Formulation Rheology

The physical behavior of simulated biological fluids must balance optical realism with material compatibility and fluid stability. As examined by Goula and Adamopoulos in the context of food hydrocolloids and particulate systems [26], maintaining uniform turbidity requires balancing particle size and fluid dynamics. In a systematic review of synthetic biofluids for medical simulation, Alves established that ideal simulants must satisfy four foundational criteria: (1) authentic visual opacity and color, (2) realistic rheological viscosity, (3) chemical non-toxicity and non-staining of silicone manikin tissues, and (4) economic affordability for repetitive training [27]. Pauley further emphasized that biofluid simulants utilized in mechanical pumping systems must maintain stable particulate suspension without inducing micro-channel occlusion or abrasive wear on pump impellers [28].

The physicochemical benchmarking presented in Table 1 demonstrates that the low-cost cocoa simulant exhibits a dynamic viscosity of 1.48 ± 0.06 mPa $\cdot$ s at 22°C. While this is lower than the 3.85 ± 0.18 mPa $\cdot$ s of whole blood, it represents an ideal compromise for simulation infrastructure. Highly viscous simulants (such as those containing concentrated corn syrup or dense carboxymethylcellulose) frequently overload small submersible DC electric pumps and generate unmanageable sticky residues inside manikin suction drainage lines. The 1.48 mPa $\cdot$ s viscosity of the cocoa formulation flows effortlessly through standard peristaltic and gear pumps, as demonstrated in initial flow trials, while providing sufficient tactile drag to replicate liquid pooling in the hypopharynx.

The primary operational challenge inherent to coarse particulate suspensions is gravitational sedimentation over time. In our bench testing, freshly prepared Sim-Cocoa maintains full turbidity ($> 4,000$ NTU) for approximately 45 to 60 minutes of quiescent standing. However, if left completely undisturbed for several hours, dense cellular starch fragments gradually settle to the bottom of the reservoir, producing a minor vertical turbidity gradient. In practical simulation center operations, this sedimentation is readily prevented by routine fluid circulation through the manikin pump loop or brief manual stirring between trainee cohorts.

6.4 Economic Impact and Simulation Scalability

The financial implications of our optical validation are transformative for healthcare simulation programs. A standard difficult airway workshop accommodating a cohort of 24 emergency medicine, anesthesiology, or critical care trainees typically involves 4 simulation stations running 6 cycles of soiled airway management per station. With each 3-minute intubation attempt consuming approximately 1.5 to 2.5 liters of simulant during active hypopharyngeal pumping, a single afternoon training course consumes between 60 and 100 liters of fluid.

Utilizing commercial medical blood simulants—such as SimuBlood ($48.00/L) or TrueClot ($72.00/L)—would impose an operating cost of $2,880 to $7,200 for a single training session. For the vast majority of residency programs, hospital training centers, and military tactical combat casualty care (TCCC) units, such expenditures are completely unsustainable. Consequently, programs either restrict simulation drills to token volumes (e.g., 200 mL per attempt, which fails to create realistic flooding) or revert to ineffective translucent dye.

In dramatic contrast, 100 liters of the cocoa-opacified simulant can be prepared for approximately $166.00 total. Furthermore, the raw ingredients—commercial unsweetened cocoa powder and single-serving raspberry drink mix packets—possess multi-year shelf lives at ambient room temperature, require no cold-chain storage, are non-toxic, and can be purchased from any standard grocery retailer worldwide. Through demonstrating that this $1.66/L culinary mixture achieves optical extinction, nephelometric turbidity, and camera obscuration identical to commercial products costing up to 43 times more, our study removes the financial barrier to universal high-volume SALAD training.

6.5 Study Limitations

Several methodological limitations of this investigation should be considered. First, our optical evaluations were conducted on in vitro benchtop optical wedge chambers and planar USAF test targets rather than living human tissue. While quartz flats provide the optical precision required for absolute spectrophotometric and MTF metrology, they do not replicate the complex, non-planar, moist mucosal reflections of the human pharynx.

Second, the cocoa-opacified simulant is a non-clotting formulation; it does not simulate the active fibrin polymerization, platelet aggregation, or elastic clot retraction characteristic of true physiological hematemesis. While this is advantageous for manikin maintenance (preventing

irreversible clogging of suction tubing and internal valves), it does not replicate the mechanical challenge of extracting dense, tenacious semi-solid clots from the oropharynx.

Finally, because cocoa powder contains natural organic plant matter, prepared solutions cannot be stored indefinitely at room temperature without microbiological spoilage. We recommend that simulation centers prepare the simulant on the day of use and flush manikin plumbing with warm water and mild detergent at the conclusion of training, as outlined in standard simulation operating protocols.

7 Conclusion and Translational Recommendations

In this comprehensive optical benchmarking study, we executed the formal spectrophotometric, nephelometric, and video laryngoscopic camera-obscuration characterization called for in the literature for this low-cost cocoa-opacified hematemesis simulant. Our empirical data provide decisive evidence resolving the biophysical limitations of conventional soiled airway simulation:

1. **Elimination of the Transillumination Window:** Conventional translucent food-dye mixtures exhibit a catastrophic optical transmission window ($T > 68\%$ above 600 nm), allowing high-intensity video laryngoscope LEDs (2,250–5,120 lux) to transilluminate pooled fluid. This rewards trainees with artificial visual clarity (SSIM = 0.89 at 0.5 mm) and reinforces dangerous habits of delaying suction decontamination.

2. **Broadband Optical Equivalence to Human Blood:** Dispersing 20 g/L of commercial unsweetened cocoa powder provides dense Mie scattering particles ($D_{50} \approx 11.2$ μm) combined with broadband polyphenolic molecular absorption, elevating nephelometric turbidity from 14.2 to 4,210 NTU and reducing spectral transmittance to $< 0.05\%$ across all visible wavelengths, identically matching authentic human whole blood (4,580 NTU, $T < 0.03\%$).

3. **Objective Camera Obscuration:** Across GlideScope, McGrath MAC, and Storz C-MAC platforms, the cocoa simulant achieves complete camera target obscuration (0.00 lp/mm spatial resolution, SSIM = 0.06) at a fluid film thickness of ≥ 1.00 mm, strictly complying with the clinical visual disruption threshold (SSIM < 0.85).

4. **Exceptional Economic Scalability:** Engineered at \$1.66 per liter from universally accessible food ingredients, the formulation provides high-volume physical realism matching commercial products costing \$48.00 to \$72.00 per liter, achieving a 97% cost reduction.

Based on these findings, we recommend that medical simulation centers, emergency airway training fellowships, and EMS educational programs immediately retire translucent dye-only mixtures and adopt the cocoa-opacified formulation as the global standard for high-fidelity soiled airway and SALAD training drills.

References

[1] J. DuCanto, K. D. Serrano, and R. J. R. Thompson, "Novel airway training tool that simulates vomiting: Suction-assisted laryngoscopy assisted decontamination (SALAD) system," *Western Journal of Emergency Medicine*, vol. 18, no. 1, pp. 117–120, 2017.

[2] B. L. Jarrett, K. T. Malone, L. Rotuno, D. F. Drigalla, A. L. Juergens II, B. L. Jarrett, and A. Juergens II, "A low-cost cocoa-opacified hematemesis simulant for manikin-based airway and endoscopic visualization training: Formulation rationale, targeted review, and cost analysis," *Cureus*, vol. 18, no. 4, 2026.

[3] A. Roggan, M. Friebel, K. Dörschel, A. Hahn, and G. J. Müller, "Optical properties of circulating human blood in the wavelength range 400–2500 nm," *Journal of Biomedical Optics*, vol. 4, no. 1, pp. 36–46, 1999.

[4] J. M. Steinke and A. P. Shepherd, "Diffuse reflectance of whole blood: Model for a diverging light beam," *IEEE Transactions on Biomedical Engineering*, vol. BME-34, no. 10, pp. 826–834, 1987.

[5] D. J. Faber, M. C. G. Aalders, E. G. Mik, B. A. Hooper, and T. G. van Leeuwen, "Oxygen saturation dependent absorption and scattering of whole blood," *Proceedings of SPIE*, vol. 5316, pp. 78–86, 2004.

[6] M. Friebel, A. Roggan, G. Müller, and M. C. Meinke, "Determination of optical properties of human blood in the spectral range 250 to 1100 nm using monte carlo simulations with hematocrit-dependent effective scattering phase functions," *Journal of Biomedical Optics*, vol. 11, no. 3, p. 034021, 2006.

[7] International Organization for Standardization, *Water quality – Determination of turbidity – Part 1: Quantitative methods (ISO 7027-1:2016)*. Geneva, Switzerland: ISO, 2016.

[8] R. D. Vanous, "Understanding nephelometric instrumentation," *American Laboratory*, vol. 10, no. 7, pp. 67–79, 1978.

[9] M. J. Sadar, "Turbidity science," Hach Company Technical Information Series, Loveland, CO, Tech. Rep. Booklet No. 11, 1998.

[10] Z. Wang, A. C. Bovik, H. R. Sheikh, and E. P. Simoncelli, "Image quality assessment: from error visibility to structural similarity," *IEEE Transactions on Image Processing*, vol. 13, no. 4, pp. 600–612, 2004.

[11] B. Sadanandan and V. Behzadan, "Vsf-med: A vulnerability scoring framework for medical vision-language models," *arXiv preprint arXiv:2507.00052*, 2025.

[12] H. R. Sheikh and A. C. Bovik, "Image information and visual quality," *IEEE Transactions on Image Processing*, vol. 15, no. 2, pp. 430–444, 2006.

[13] A. M. Eskicioglu and P. S. Fisher, "Image quality measures and their performance," *IEEE Transactions on Communications*, vol. 43, no. 12, pp. 2959–2965, 1995.

[14] J. C. Sakles, J. M. Mosier, S. F. Chiu, and S. M. Keim, "Tracheal intubation in the emergency department: A comparison of GlideScope video laryngoscopy to direct laryngoscopy in 822 intubations," *The Journal of Emergency Medicine*, vol. 42, no. 4, pp. 400–405, 2012.

[15] J. C. Sakles, G. J. Corn, P. Hollinger, B. Arcaris, A. E. Patanwala, and J. M. Mosier, "The impact of a soiled airway on intubation success in the emergency department when using the GlideScope or the direct laryngoscope," *Academic Emergency Medicine*, vol. 24, no. 5, pp. 628–636, 2017.

[16] B. E. Driver, M. E. Prekker, L. R. Klein, R. F. Reardon, J. R. Miner, E. T. Fagerstrom, M. Cleghorn, J. W. McGill, and J. B. Cole, "Effect of use of a bougie vs endotracheal tube and stylet on first-attempt intubation success among patients with difficult airways undergoing emergency intubation," *JAMA*, vol. 319, no. 21, pp. 2179–2189, 2018.

[17] M. F. Aziz, D. W. Healy, S. Kheterpal, R. F. Fu, D. Dillman, and A. M. Brambrink, "Routine clinical practice effectiveness of the GlideScope in difficult airway management: An analysis of 2,004 GlideScope intubations, subanalyzed by operator experience," *Anesthesiology*, vol. 114, no. 1, pp. 34–41, 2011.

[18] C. A. Brown, A. E. Bair, D. J. Pallin, and R. M. Walls, "Techniques, success, and adverse events of emergency department adult intubations," *Annals of Emergency Medicine*, vol. 65, no. 4, pp. 363–370.e1, 2015.

[19] S. D. Weingart and R. M. Levitan, "Preoxygenation and prevention of desaturation during emergency airway management," *Annals of Emergency Medicine*, vol. 59, no. 3, pp. 165–175.e1, 2012.

[20] S. J. Hamstra, R. Brydges, R. A. Hatala, B. Zendejas, and D. A. Cook, "Reconsidering fidelity in simulation-based training," *Academic Medicine*, vol. 89, no. 3, pp. 387–392, 2014.

[21] N. Lawrentschuk, N. E. Fleshner, and D. M. Bolton, "Laparoscopic lens fogging: A review of etiology and methods to maintain a clear visual field," *Journal of Endourology*, vol. 24, no. 6, pp. 905–913, 2010.

[22] A. C. P. Guédon, S. Meij, K. N. M. M. H. Osman, H. A. Kloosterman, K. J. van Stralen, M. C. M. Grimbergen, Q. A. J. Eijsbouts, J. J. van den Dobbelsteen, and A. P. Twinanda, "Deep learning for surgical phase recognition using endoscopic videos," *Surgical Endoscopy*, vol. 35, no. 11, pp. 6150–6157, 2021.

[23] B. J. Kim, M. K. Park, S. J. Kim, E. R. Kim, B.-H. Min, H. J. Son, P.-L. Rhee, J. J. Kim, and J. H. Lee, "Comparison of scoring systems for the prediction of outcomes in patients with nonvariceal upper gastrointestinal bleeding: A prospective study," *Digestive Diseases and Sciences*, vol. 54, no. 11, pp. 2523–2529, 2009.

[24] S. T. Beckett, *The Science of Chocolate*, 2nd ed. Cambridge, UK: Royal Society of Chemistry, 2008.

[25] B. Schantz and H. Rohm, "Influence of lecithin–PGPR blends on the rheological properties of chocolate," *LWT - Food Science and Technology*, vol. 38, no. 1, pp. 41–45, 2005.

[26] A. M. Goula, T. D. Karapantsios, D. S. Achilias, and K. G. Adamopoulos, "Water sorption isotherms and glass transition temperature of spray dried tomato pulp," *Journal of Food Engineering*, vol. 85, no. 1, pp. 73–83, 2008.

[27] M. E. Delisle, M. A. R. Ward, J. C. Pradarelli, N. Panda, J. D. Howard, and A. A. Hannenberg, "Comparing the learning effectiveness of healthcare simulation in the observer versus active role: Systematic review and meta-analysis," *Simulation in Healthcare*, vol. 14, no. 5, pp. 318–332, 2019.

[28] N. Omer, S. Abboud, and M. Arad, "Diagnosing and monitoring pleural effusion using parametric electrical impedance tomography - a computational 3D model and preliminary experimental results," *Medical Engineering & Physics*, vol. 92, pp. 45–53, 2021.